



Ultrafast superconducting single-photon detector

G. Goltsman , A. Korneev , A. Divochiy , O. Minaeva , M. Tarkhov , N. Kaurova , V. Seleznev , B. Voronov , O. Okunev , A. Antipov , K. Smirnov , Yu. Vachtomin , I. Milostnaya & G. Chulkova

To cite this article: G. Goltsman , A. Korneev , A. Divochiy , O. Minaeva , M. Tarkhov , N. Kaurova , V. Seleznev , B. Voronov , O. Okunev , A. Antipov , K. Smirnov , Yu. Vachtomin , I. Milostnaya & G. Chulkova (2009) Ultrafast superconducting single-photon detector, Journal of Modern Optics, 56:15, 1670-1680, DOI: [10.1080/09500340903277750](https://doi.org/10.1080/09500340903277750)

To link to this article: <http://dx.doi.org/10.1080/09500340903277750>



Published online: 06 Jan 2010.



Submit your article to this journal [↗](#)



Article views: 173



View related articles [↗](#)



Citing articles: 15 View citing articles [↗](#)

Ultrafast superconducting single-photon detector

G. Goltsman, A. Korneev*, A. Divochiy, O. Minaeva, M. Tarkhov, N. Kaurova, V. Seleznev, B. Voronov, O. Okunev, A. Antipov, K. Smirnov, Yu. Vachtomin, I. Milostnaya and G. Chulkova

Department of Physics and Information Technology, Moscow State Pedagogical University, 1 Malaya Pirogovskaya, Moscow 119991, Russia

(Received 4 February 2008; final version received 19 August 2009)

The state-of-the-art of the NbN nanowire superconducting single-photon detector technology (SSPD) is presented. The SSPDs exhibit excellent performance at 2 K temperature: 30% quantum efficiency from visible to infrared, negligible dark count rate, single-photon sensitivity up to $5.6\ \mu\text{m}$. The recent achievements in the development of GHz counting rate devices with photon-number resolving capability is presented.

Keywords: superconducting single-photon detectors; thin superconducting NbN films; infrared detectors

1. Introduction

Recently the interest in infrared single-photon detectors (SPD) has increased dramatically. Many scientific and technical applications ranging from study of single-photon emitters to quantum cryptography and quantum computing would benefit from high sensitive and fast SPD. Typically such applications require that a SPD combines several of the following parameters: picosecond timing resolution, GHz counting rate, low dark counts rate and rather high quantum efficiency (QE) especially at standard telecom wavelength of $1.55\ \mu\text{m}$. Meanwhile, commercially available semiconductor Si and InGaAs avalanche photodiodes (APD) do not meet those requirements. Although the best Si APDs [1] have 40 ps timing resolution, $\approx 10\ \text{s}^{-1}$ dark counts rate, and maximum count rate about 3 MHz, their operational wavelength range is restricted by the energy gap in Si and thus their quantum efficiency drops rapidly at wavelength longer than $1.1\ \mu\text{m}$ making them unavailable for applications at telecom wavelengths. InGaAs APDs [2] have a wider wavelength band, up to $1.8\ \mu\text{m}$, but they have worse timing resolution ($\approx 300\ \text{ps}$) and suffer from very high dark counts rate ($10^4\ \text{s}^{-1}$). Besides, both types of APDs need electrical quenching for fast operation.

The most promising competitors of the APDs are the superconducting detectors. They are very attractive due to low noise operation at cryogenic temperature, very high sensitivity and capability to count photons of middle infrared range (up to $5\ \mu\text{m}$ wavelength). The transition edge sensor (TES) is well known and has

well-established technology. Although these devices were reported to have almost unity quantum efficiency at $1.55\ \mu\text{m}$ they are very slow (20 kHz maximum counting rate), have submicrosecond timing resolution and require an operational temperature $\approx 0.1\ \text{K}$. Being capable of counting infrared photons and having no intrinsic dark counts [3], they are susceptible to triggering by mid-infrared photons.

Several years ago a novel type of SPD was introduced: a superconducting single-photon detector (SSPD) made from ultrathin NbN film [4]. Although this type of detector is quite young it has already demonstrated very promising capabilities. Up to 30% quantum efficiency was measured in near infrared ($1.3\ \mu\text{m}$ wavelength) at 2 K temperature and single-photon sensitivity up to $5.6\ \mu\text{m}$ [5], very low level of dark counts [6], and timing resolution of 18 ps [7].

Because of the favorable characteristics and the possibility to be effectively coupled to single-mode optical fiber [8,9] as well as an installation into a closed cycle refrigerator system [10] many applications of the SSPD have already been reported. The most impressive one is the report on the quantum key distribution (QKD) over 200 km distance [11]. Other QKD experiments also were reported in [12] as well as non-quantum optical communication [13]. The implementation of the SSPD for the research into emission of single-photon sources, e.g. quantum dots or quantum wells, by time-correlated single-photon counting methods were reported as well [9,14–16]. Recently several experiments on quantum information processing with SSPD have been reported [17,18].

*Corresponding author. Email: kr78@mail.ru

In this paper we give an overview of the state-of-the-art SSPD technology: fabrication and characterization as well as novel results of the development of the ultrafast SSPD which combines GHz counting rate with photon number resolving capability. We also present here a double channel receiver system which is equipped with two fiber-coupled SSPDs.

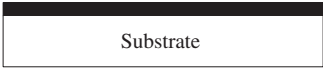

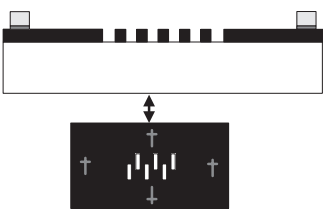

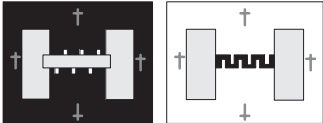
2. SSPD fabrication process

The SSPD fabrication process was described in detail in [19], here we give a brief description. NbN superconducting films used for fabrication of SSPDs have a thickness 3.5–4 nm and are deposited on R-cut sapphire substrates by a DC reactive magnetron sputtering in an Ar and N₂ mixture. The film characteristics are as follows: surface resistance $R_s=380\text{--}500\ \Omega\ \text{sq}^{-1}$, critical temperature $T_c=10\text{--}11\ \text{K}$, superconducting transition width $\Delta T_c \approx 0.3\ \text{K}$, and critical current density $j_c=3\text{--}5 \times 10^6\ \text{A cm}^{-2}$ at 4.2 K. Details of our

thin NbN film fabrication process is described in detail in [20]. During the NbN deposition process, the substrate is heated up to 800°C. The SSPD is patterned in a long stripe that covers $10\ \mu\text{m} \times 10\ \mu\text{m}$ area and has the filling factor (the ratio of the area occupied by the superconducting meander to the device nominal area) up to 0.6. The width of superconductive stripe is 120 nm. The film is patterned by a direct electron beam lithography and reactive ion etching.

Table 1 shows the sequence of technological operations in the process and lists their main characteristics. Note that in this case the areas under which the superconductor is removed are exposed in the resist during electron beam lithography. The minimal width of the superconducting stripe does not depend directly on electron beam diameter rather, it is largely determined by scattering in the photoresist. We used the resist PMMA 950K that was later removed from the superconductor using the reactive ion etching process. Figure 1 shows the SSPD chip with gold contact pads

Table 1. Technological process of SSPD fabrication using direct electron beam lithography and reactive ion etching process.

ID	Sketch	Comments
1. Deposition of a NbN film by DC reactive magnetron sputtering.		Substrate: double-side-polished, 300 μm thick sapphire. Residual pressure 1.5×10^{-6} mbar. Substrate temperature 800°C. N ₂ partial pressure 10^{-4} mbar. Ar partial pressure 5×10^{-3} mbar.
2. Patterning of alignment marks		Lift-off process. Ti/Au 5/100 nm alignment marks. Vacuum resistive evaporation at room temperature. Optical lithography process with AZ1512 photoresist.
3. Patterning of stripe windows in preparation for a meander structure.		Direct electron beam lithography process with PMMA 950K (2%, 0.08 μm) electron resist. Process parameters: $I=25\ \text{pA}$, $U=25\ \text{kV}$. The developer: toluene and isopropanol 1:10 mixture. Reactive ion etching of NbN film in SF ₆ . Removal of electron resist layer.
4. Patterning of outer contact pads.		Lift-off process. Ti/Au 5/200 nm contact pads. Vacuum resistive evaporation at room temperature. Optical lithography process with AZ1512 photoresist.
5. Final patterning of meander structure.		Photolithography process with AZ1512 photoresist. Chemical etching of unprotected areas of NbN film in CP-4 (HNO ₃ /HF/CH ₃ COOH (5:3:3)). Removal of electron resist layer.

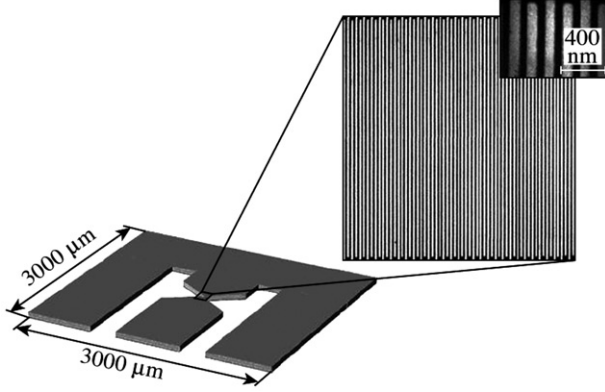


Figure 1. Overall view of the SSPD chip and the SEM image of the NbN meander. The width of superconducting stripe is 120 nm, meander filling factor is 0.6.

for connection to co-planar line and SEM image of the NbN meander.

3. State-of-the-art SSPD performances

For SSPD characterization we used both fiber-based setup and setup with free-space propagating beam. As the light sources we used light emitting diodes and an infrared grating spectrometer. The SSPD was mounted either in a dipstick and emerged in liquid helium or in a vacuum optical cryostat. The bias current was fed to the SSPD from a DC source with internal resistance in the range 20–100 Ω . Taking into account the fact that SSPD resistance after photon absorption is several hundreds of ohms, the SSPD is operated in a regime similar to the constant-voltage regime. The SSPD can be operated without an external reset as superconductivity is spontaneously restored. Upon photon absorption SSPD produces a distinct voltage pulse with an amplitude of 0.3 mV by the order of magnitude, which is fed through a bias-T to amplifiers and then to an oscilloscope and a pulse counter. The pulse amplitude

does not depend on the photon energy but is proportional to the SSPD bias current.

We define quantum efficiency QE as the ratio of the SSPD photoresponse counts N_{reg} to the number of photons N_{inc} falling on the SSPD active area of $10 \mu\text{m} \times 10 \mu\text{m}$:

$$QE = \frac{N_{\text{reg}}}{N_{\text{inc}}}. \quad (1)$$

The value of N_{reg} was directly measured by the read-out electronics (if the dark counts rate R_{dk} cannot be neglected compared to N_{reg} then N_{reg} is taken as a difference of total count rate and dark counts rate). The N_{inc} was derived from the power measurements in the fiber-based setup.

Even when SSPD input is completely blocked from radiation by cold shields it produces spontaneous voltage pulses similar to the photoresponse pulses. We identify them as dark counts and their rate R_{dk} is defined as the mean number of the SSPD response pulses occurring during 1 s. To improve the accuracy of the measurements, the SSPD was shielded by a metal film with the temperature of ambient liquid helium. Without shielding the parasitic thermal background radiation could manifest itself as the excessive dark counts.

The trade-off between the QE and R_{dk} we describe in terms of noise equivalent power NEP , which is defined for quantum detectors as

$$NEP = \frac{h\nu}{QE} (2R_{\text{dk}})^{1/2} \quad (2)$$

where $h\nu$ is the photon energy. To determine the NEP , we used experimentally measured values of QE and R_{dk} .

In visible light and near infrared we studied SSPD QE with light emitting diodes (LED) and the light was delivered to the SSPD by a fiber [21]. In Figure 2(a), we present QE versus normalized bias current I_b/I_c

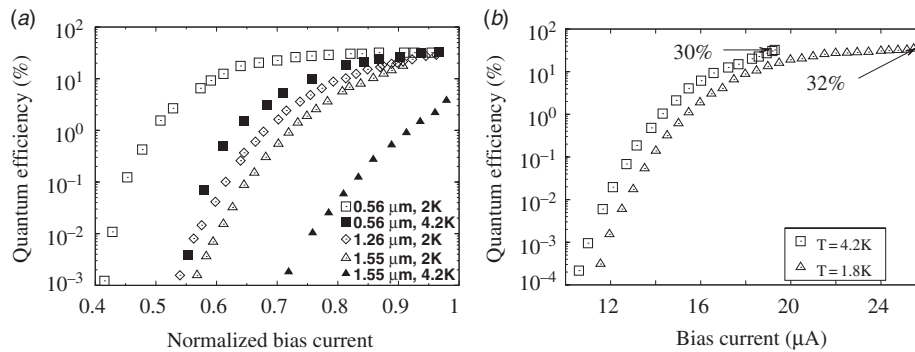


Figure 2. Quantum efficiency of the SSPD versus normalized bias current I_b/I_c measured at 2.0 K (open symbols) and 4.2 K (solid symbols) temperatures and different wavelengths (a). Typically, an increase of quantum efficiency with temperature reduction is observed. Conversely, for the best SSPD (b) at 1.26 μm wavelength QE does not increase with the reduction of operation temperature from 4.2 K (squares) to 1.8 K (triangles).

measured at 0.56, 1.26, and 1.55 μm wavelengths for two operating temperatures: 4.2 and 2.0 K. One can see that in the visible range QE reaches 30% already at a temperature of 4.2 K, whereas in near infrared at 1.55 μm wavelength QE is only about 4% at 4.2 K. The reduction of operation temperature typically leads to significant improvement of the SSPD QE , i.e. it reaches 30% at 1.26 μm wavelength and 17% at 1.55 μm at 2.0 K temperature. At the same time, advances in the fabrication technology allowed us to produce rare SSPDs that reach $QE=30\%$ at 4.2 K and do not exhibit any increase in QE with temperature reduction at all. For example, Figure 2(b) presents QE versus I_b for such an SSPD. Although such devices are very rare presently, they are very attractive for implementation in cryocooler systems (since 4 K cryocoolers are cheaper and easier to fabricate than 2 K cryocoolers). Further improvement of the fabrication process will increase the fabrication yield of such SSPDs and make them commercially available.

In [22] a direct measurement of the NbN film patterned in a similar manner to SSPD structures is presented. It was reported that the maximum absorption cannot exceed 30%. That means that SSPD detects every near infrared photon absorbed by the film. Further improvement of the QE is possible only with SSPD integration in a $\lambda/4$ -microcavity. This was independently performed by Milostnaya et al. [23] and Rosfjord et al. [24] and $QE \approx 60\%$ was reported [24].

We studied SSPD broadband spectral sensitivity with a grating spectrometer and the light was delivered in free space to the SSPD installed in the optical cryostat [21]. We observed single-photon response in all the investigated spectral range which was from 0.56 to 5.6 μm . We believe that SSPD is capable of single-photon counting even at longer wavelength but we were limited by our equipment to prove it in the experiment. Figure 3(a) presents QE versus wavelength measured at a temperature of 3 K and different bias currents in the range 0.78 to 0.94 of I_c . At each

wavelength the SSPD was checked for single-photon response (especially in mid-IR) by checking the linearity of photon count rate versus the number of incoming photons.

We also thoroughly investigated SSPD's QE at 5 μm wavelength and its dependence on the temperature [25]. As a light source we used an LED installed in the cryostat. The LED power was measured using a Galley cell and was used to calculate QE . Figure 3(b) shows the temperature dependence of QE versus bias current at different temperatures. One can see a significant increase of QE with the reduction of temperature from 5 to 1.7 K. At temperatures below 2 K one can see that the dependence of QE on temperature becomes less steep compared to higher temperatures. The maximum measured QE value at 5 μm wavelength and 1.7 K temperature is 0.4%.

When completely shielded, SSPD dark counts rate R_{dk} exponentially depends on I_b/I_c (solid squares in Figure 4(a)). At a given I_b/I_c , with the temperature decrease one can observe a reduction of R_{dk} . Exponential character of R_{dk} was observed over 7 orders of magnitude. The minimum measured value of dark counts rate was as low as $2 \times 10^{-4} \text{ s}^{-1}$ and was limited by the duration of the experiment, i.e. accumulating several dark counts took about 8 h. Figure 4(a) presents R_{dk} measured at 2.0 K temperature for a SSPD coupled to single-mode optical fiber [9]. At 2.0 K temperature SSPD is sensitive to thermal background radiation which manifests itself as excessive dark counts (open triangles in Figure 4(a)). When we applied a cold filter to cut-off the thermal photons the dark counts rate was noticeably reduced (solid triangles in Figure 4(a)).

An optimal operation regime of the SSPD is a trade-off between the high QE and the low R_{dk} . Maximum QE values correspond to rather high ($\approx 10^3$ counts per second and more) dark-count rates. This trade-off is quantitatively expressed in terms of noise equivalent power NEP . Calculation results for the SSPD NEP based on experimentally measured QE and

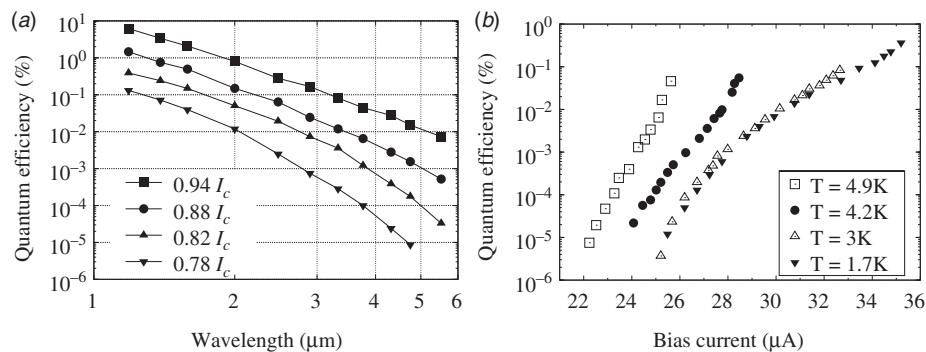


Figure 3. Spectral sensitivity (QE versus wavelength) of SSPD at a temperature of 3 K and different bias currents in the range 0.78 to 0.94 of I_c (a) and QE versus bias current for 5 μm wavelength at different temperatures in the range 4.9–1.7 K (b).

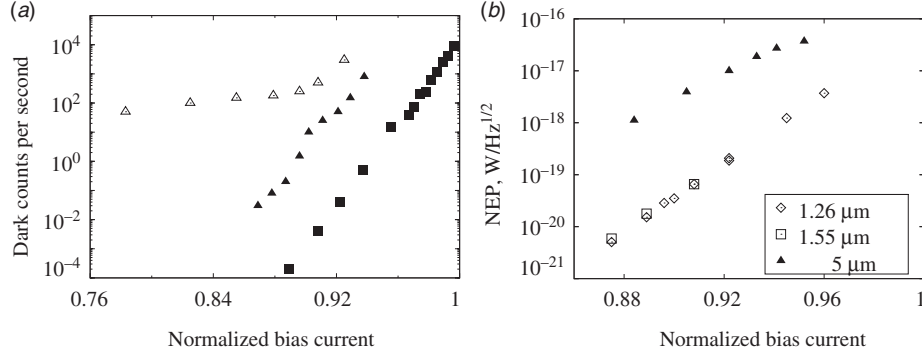


Figure 4. The dark counts rate (a) versus normalized bias current I_b/I_c for single-mode fiber coupled SSPD without a filter (open triangles), with a filter (solid triangles) to block thermal background radiation, and when SSPD is completely shielded (solid squares). The noise equivalent power NEP (b) measured at 1.26 and 1.55 μm at a temperature of 2 K and at 5 μm wavelength calculated from QE measured at 1.7 K and dark counts rate measured at a temperature of 2 K when the SSPD is completely shielded.

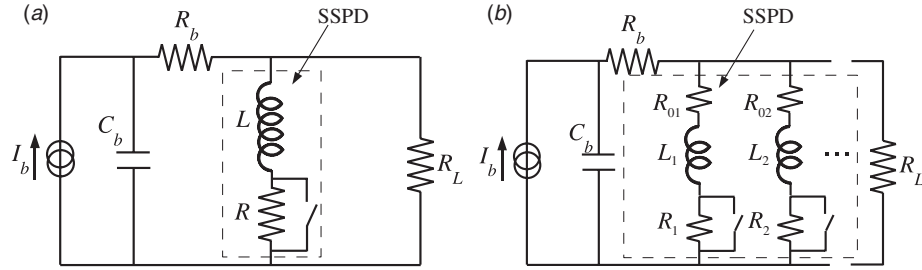


Figure 5. SSPD equivalent circuit of standard single-wire SSPD (a) and novel 'parallel' wire SSPD (b).

R_{dk} are presented in Figure 4(b). We used QE measured at 1.26 and 1.55 μm wavelength at a temperature of 2.0 K and QE for 5 μm wavelength measured at 1.7 K. R_{dk} was taken from the plot in Figure 4(a) (solid squares). At 2.0 K, the QE reaches 10% for the telecommunication wavelengths of 1.3 and 1.55 μm , simultaneously, the NEP reaches a level as low as $5 \times 10^{-21} \text{ W Hz}^{-1/2}$. At the wavelength of 5 μm , the NEP is $1 \times 10^{-18} \text{ W Hz}^{-1/2}$. To our knowledge, this is the best middle infrared performance for any currently available single-photon detector.

4. Kinetic inductance limitation and GHz counting rate SSPD

4.1. How to reduce the kinetic inductance

Early measurements performed with single strips and short meander structures covering an area of $4 \mu\text{m} \times 4 \mu\text{m}$ made from 10 nm thick NbN film showed a response time of about 150 ps with the pulse-to-pulse jitter as low as 18 ps [6,7,26]. Nevertheless, high quantum efficiency devices made from 3.5 nm thick NbN film and covering $10 \mu\text{m} \times 10 \mu\text{m}$ area with about 50% filling factor exhibited significantly longer response time, typically several nanoseconds. In [27] Kerman et al. showed that large active area SSPDs suffer from a

significant kinetic inductance which limits their photo-response to the nanosecond time range. The kinetic inductance is a manifestation of the kinetic energy of the electrons accelerated by the electric field [28]. In normal metal, due to low kinetic energy of electrons kinetic inductance is negligibly small compared to the well-known magnetic field inductance. In superconductors, conversely, the kinetic energy of the superconducting electrons can be much higher than in normal metal and there are cases when the kinetic inductance cannot be neglected. For a superconducting film with thickness d , width w , and length l the kinetic inductance is given by

$$L_K = \frac{\mu_0 \lambda_L^2 l w}{d}, \quad (3)$$

where λ_L is the effective London penetration depth.

Figure 5(a) shows an equivalent circuit of the kinetic-inductance-limited SSPD together with a DC bias source and a 50 Ω transmission line R_L . In our experiment bias-T was always placed on the same holder with the SSPD. It consisted of a resistor R_b in 20–100 Ω range and a capacitor C_b of about 1000 pF. The DC source could be treated as a voltage source on a subnanosecond time scale. Placing the bias-T near the SSPD allowed us to provide an immediate response of the biasing circuit to the change of SSPD resistance

(without any delays connected with the signal propagation along the transmission line). SSPD can be treated as an inductance L connected in series to a resistor R and a switch. The resistance R corresponds to the resistance of the SSPD after photon absorption. Since only a small portion of the nanowire undergoes the superconducting-to-normal transition, a typical value of R is several hundreds of ohms. When SSPD is in the superconducting state the switch is closed. The absorption of a photon with subsequent formation of the resistive region may be treated as the opening of the switch. As the resistance R is several times higher than the resistance of R_b and R_L one may consider that the current through the SSPD drops (and simultaneously the voltage on the SSPD terminals rises) following an exponential law with the characteristic time L_{kin}/R . When the resistive region disappears and the superconductivity restores we may think that the switch is closed. Due to kinetic inductance the current through the SSPD does not increase immediately, but with the characteristic time $\tau = L_{\text{kin}}(R_b + R_L)/(R_b R_L)$ (the resistors R_b and R_L are connected in parallel). The same is true for the voltage on the SSPD terminals. It drops obeying an exponential law with the same characteristic time τ . As R is several times higher than $(R_b R_L)/(R_b + R_L)$, the rise time is several times shorter than the fall time.

To reduce the characteristic times we proposed to divide one long meander into several sections of equal length and connect them in parallel. All sections are placed close to each other and cover the same square area of $10\mu\text{m} \times 10\mu\text{m}$. An equivalent circuit diagram for such ‘parallel’ nanowire SSPD is presented in Figure 5(b). When a photon is absorbed in one of the sections that section becomes resistive. Although at first glance it seems that other sections should act like a shunt, this does not actually happen due to the kinetic inductance of those sections. Resistors R_b and R_L correspond to the resistances of the bias source and the transmission line, respectively. Inductances L_1, L_2, \dots represent kinetic inductances of each meander-shaped section whereas resistors R_1, R_2, \dots denote the resistances of the sections after photon absorption. For a device consisting of N parallel sections the inductance of a single section is N times smaller than the inductance of the large $10\mu\text{m} \times 10\mu\text{m}$ meander. Since the sections are connected in parallel the overall relaxation characteristics time τ will be N^2 times smaller, and already for $N=5$ and above it will be in the subnanosecond range.

After the formation of the resistive region in one section the bias current of that section starts dropping. Simultaneously the currents in other sections start to grow. For proper operation the bias current of the sections should be selected so that the maximum

current does not exceed the critical current of the section. Otherwise, the increasing current may exceed the critical current of a single strip and will switch it to the resistive state too. The more sections we have the smaller the increase of the current in other sections. The value of the excess current can be reduced if a resistor is connected in series to the nanowire (R_{01}, R_{02}, \dots in Figure 5(b)) allowing operation closer to the critical current and, as a consequence, providing higher QE . From the numerical simulation of the circuit, we estimated these serial resistances which should be in the range 1–100 ohm depending on the number of parallel meander sections.

It is important to note that the development of low kinetic inductance SSPD solely for the reduction of the electrical pulse duration is not of much importance since the pulse width can be reduced easily by means of electronics. What is more the reset time of the SSPD, which is affected by its kinetic inductance, is important. Indeed, since the quantum efficiency is strongly dependent on the bias current (see Figure 2) it is important to reduce the time needed for the bias current to restore its original value after the photon absorption, in other words, to reduce the time required for the QE to reach its initial value.

4.2. Low kinetic inductance SSPD fabrication

The basic idea in ‘parallel’ nanowire SSPD fabrication is to use the already developed process of the single-meander SSPD fabrication (which is described above). Figure 6(a) presents the SEM image of the ‘parallel’ SSPD, the inset shows the meander with a 120 nm wide NbN strip. Figure 6(b) shows a sketched drawing with the arrows showing the directions of the bias current flow. The first step is the e-beam patterning of the straight lines from which the NbN film will be removed and that will form the future meanders (grey in Figure 6(b)). This step is the most important for high quality SSPD fabrication and it is performed absolutely in the same way as it was with the traditional SSPDs. The second step is the patterning of the parallel meander wiring (white areas in the Figures 6(a) and (b)). Then the planar resistors are formed from 30 nm thick gold film. Varying their length and width, as well as the thickness of the gold film we can vary their resistance. For a five-section SSPD we used resistors with a size of $0.5\mu\text{m} \times 20\mu\text{m}$ and having a resistance of about 100 Ω . Finally, the film around the meanders and their wiring are removed forming the completed ‘parallel’ SSPD device. Being patterned in the same way as we did for the conventional single-meander SSPDs, they are expected to have the same high quantum efficiency.

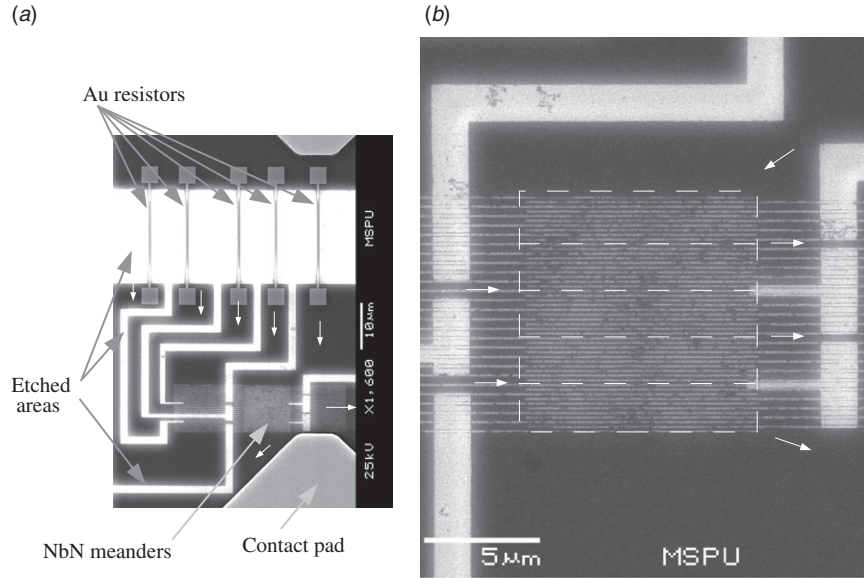


Figure 6. SEM image of the ‘parallel’ nanowire SSPD (a) and SEM of its central part with NbN meanders (b), small white arrows show the directions of current flow, dashed white rectangles surround each meander.

4.3. Parallel-wire SSPD characterization

We characterized photoresponse time for the ‘parallel’ nanowire SSPDs by direct measurements of waveform transients with the single-shot and sampling oscilloscopes. As the light sources we used a $1.26\text{ }\mu\text{m}$ cw light emitting diode and a 850 nm GaAs pulsed laser operated at 100 kHz rate and producing 30 ps wide light pulses. We studied SSPDs consisting of 1, 2, 5 and 12 nanowires connected in parallel. For all the SSPDs the total area covered by the nanowires was $10\text{ }\mu\text{m} \times 10\text{ }\mu\text{m}$.

In Figure 7 we plotted the characteristic fall times (which we define as $1/e$) for 1, 2, 5, and 12 nanowire devices which were 10 ns , 2.5 ns , 450 ps , and 150 ps , respectively [29]. We also plotted the $1/N^2$ law (solid line) which fall times should obey. One can see that all

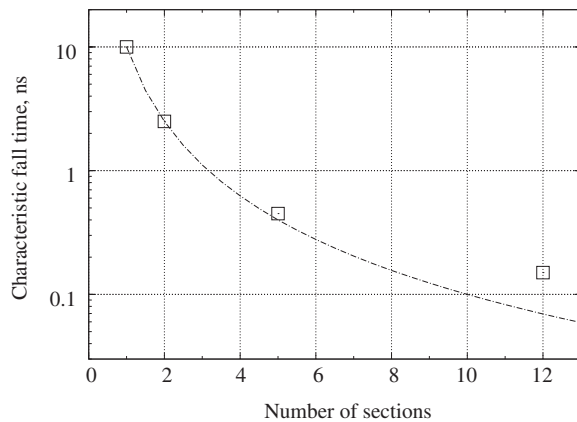


Figure 7. Characteristic fall time versus number of parallel wires (measured as $1/e$), the solid curve is the $1/N^2$ fit with the kinetic inductance $L_0 \approx 500\text{ nH}$.

the devices except the 12-wire SSPD follow this law. From the $1/N^2$ fitting curve in Figure 7 we can estimate the kinetic inductance of a one-section SSPD to be equal to $\approx 500\text{ nH}$ which is in a reasonable agreement with the results reported in [27] for similar devices. As for a 12-nanowire device, its fall time is neither limited by the kinetic inductance nor by the characteristic energy relaxation times in NbN film which are in the tens of picoseconds range [30]. One can expect that such ultra-short pulses are significantly affected by the intrinsic dynamics of the resistive region. In [29] several approaches to the description of the resistive region evolution were proposed, such as hotspot thermalization with the strong influence of the Joule heating or the vortex–antivortex unbinding process. Anyway the accurate description requires further investigation.

5. Photon-number resolving SSPD

Besides subnanosecond response time the above-described ‘parallel’ nanowire SSPD is capable of resolving the number of photons falling on its surface simultaneously. Indeed, if two strips of such a device become resistive simultaneously, the portion of the bias current expelled to the transmission line will be higher (numerical simulation shows that it should be almost twice higher than in case of a single strip switch) providing a higher voltage pulse and giving a way to distinguish the number of simultaneously detected photons by the magnitude of the response voltage. Of course, if two or more photons are absorbed by the same strip they cannot be distinguished since the response magnitude does not depend on the number of

photons absorbed by one strip (like took place for single-strip SSPD). Thus, to avoid non-linear effects the number of simultaneously detected photons should be much lower than the number of parallel strips.

We performed an experimental study of the photon number resolving (PNR) capability of the new generation SSPD (PNR-SSPD). The details are reported in [31–33]. Here we give a brief overview of those results. The experimental setup consisted of a pulsed semiconductor laser (operating at $0.85\mu\text{m}$ wavelength with 30 ps pulse width and 100 kHz maximum repetition rate) whose radiation was fed into a fiber and then divided in two equal parts. One part was fed to the power meter whereas the other part was fed to the SSPD coupled to a fiber and maintained in liquid helium at a temperature of 4.2 K. The electrical photoresponse pulse was fed to a coaxial cable and then to amplifiers (500 MHz band, ≈ 70 dB amplification) and a pulse counter and an oscilloscope. The laser and the oscilloscope were triggered by a single impact generator. To vary the power of the radiation falling on the SSPD we used a variable fiber-based optical attenuator.

Four different amplitudes were easily observed. With the increase of the number of photons in the laser pulse incident on the SSPD, the probability to observe higher response amplitude increased. The proof that we really observe responses to one, two, three and four simultaneously absorbed photons was obtained from the measurement of PNR-SSPD count rates of different amplitudes versus laser pulse energy.

Assuming an ideal detector with 100% quantum efficiency, for a mean number of photons $m \ll 1$ per pulse, the probability $P(n)$ of detecting n photons from a given pulse is $P(n) \propto m^n/n!$. Consequently, the probability of detecting one photon is proportional to m , the probability of detecting two photons is proportional to m^2 , and so on. The fact that the SSPD under test had its quantum efficiency well below 100% the above treatment is in force even in a case when the number of photons falling on the SSPD is more than 1 provided that we consider actually detected photons instead of photons in the laser pulse.

Quantum efficiency QE at $1.3\mu\text{m}$ wavelength measured at a temperature of 2.2 K was $\approx 2.5\%$ and $R_{dk} \approx 0.1\text{ s}^{-1}$. This value of quantum efficiency is about an order of magnitude smaller than reported for the traditional SSPD and can be attributed to the fact that we intentionally did not take the best device for the first try at PNR-SSPD patterning. Low QE may also be attributed to the misalignment and coupling losses between the PNR-SSPD and the fiber. Meanwhile the matter of quantum efficiency is vitally important for a PNR detector. Indeed, for a detector with quantum efficiency QE the probability of n photon detection

scales as QE^n . To increase the quantum efficiency of the SSPD we propose an approach similar to the one described in [34], i.e. to integrate the SSPD with an anti-reflection coating, $\lambda/4$ cavity, and metal mirror.

6. Double-channel single-photon receiver

In [8,35] a successful fiber coupling of the SSPD was reported. In that approach a ring from photoresist was deposited on the SSPD chip ensuring alignment of the fiber against the NbN meander. In those papers the development of a two-channel fiber-coupled SSPD receiver operating in a standard storage dewar (at a temperature of 4.2 K) was reported. Here we describe a different double-channel receiver system in which we used a different method of fiber-coupling and improved the system to enable SSPD operation at a temperature of 2 K, being immersed in a transport dewar [9,16]. This system can be used for research in quantum communication and quantum optics, for example antibunching-type correlation studies of near-infrared photons emitted by semiconductor quantum dots.

The system is designed as a double-wall insert with vacuum insulation (Figure 8). Liquid helium from the storage dewar penetrates into the inner volume of the insert through the filter and the capillary. To achieve a temperature below 4.2 K the liquid helium vapor is pumped from the inner volume. The capillary limits the speed of liquid helium penetration and allows a vapor pressure of 80–120 Pa and a temperature of 1.7 K to be obtained.

The system has two identical photon detecting channels. Two SSPDs (one in each channel) are coupled to the single-mode optical fibers and mounted at the bottom of the inner volume of the insert in the liquid helium. The SSPDs are aligned against the fibers with the stand-alone micromechanical positioner and then glued to the device holder. When SSPDs are fixed in this way the positioner is removed. Electrical contact is realized through co-planar waveguides and coaxial cables connected to two room-temperature bias-Ts. For DC bias we use a home-built current/voltage source. The SSPD photoresponse voltage pulse is transmitted by the coaxial cable to the room-temperature amplifiers, one in each channel (60 dB gain) producing pulses larger than 0.5 V. Then the signals from the channels are fed to the discriminators and to the counter and oscilloscope or to the coincidence circuit depending on the goals of the experiment.

The temperature is controlled by the efficiency of pumping and is measured with the thermometer mounted on the same holder as the SSPDs. The minimum achievable temperature is mostly determined

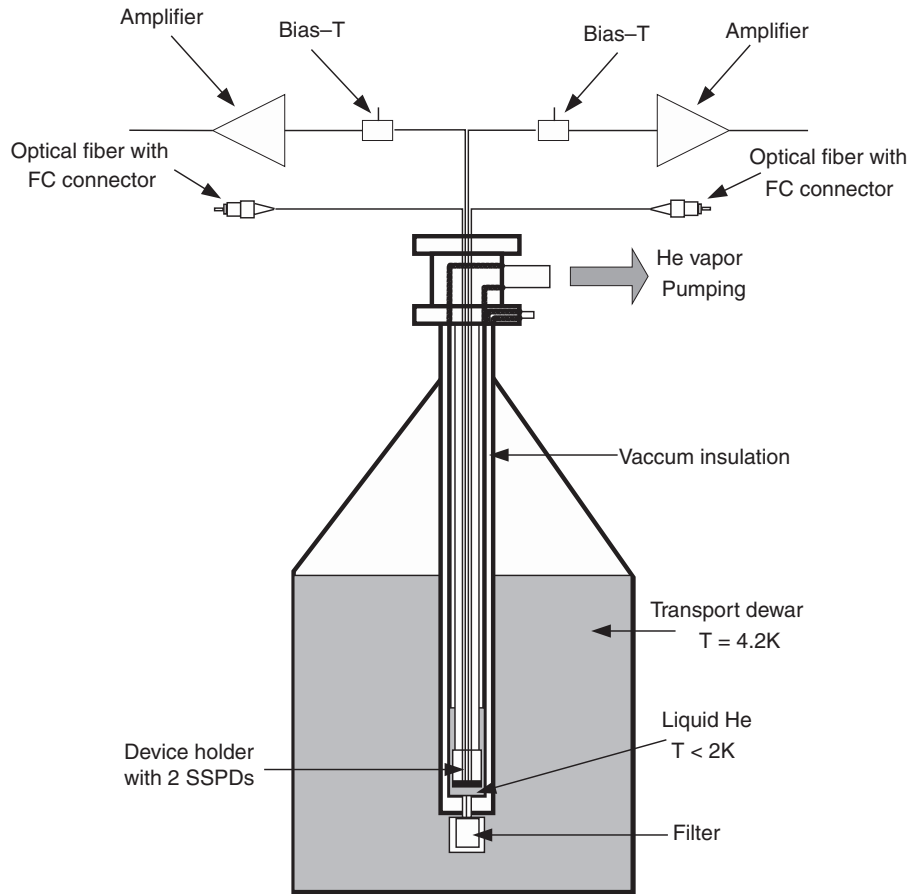


Figure 8. Double-channel single-photon receiver design.

by the capabilities of the pump and can be as low as 1.6 K. Temperature below 2 K can be achieved with a pump performance above $5 \text{ m}^3 \text{ h}^{-1}$.

In this system we implemented an optical fiber-based cold (below 77 K) filter to block the thermal background radiation from the room-temperature part of the fibers. It allowed us to achieve the system quantum efficiency (QE reduced to the input of the fiber) about 10% (at $1.26 \mu\text{m}$ wavelength) at a dark count rate of 1–2 counts per second. In many applications, this fact allows one to use SSPDs without gating, a method widely used with APD for dark count reduction. For time-correlated single-photon counting, pulse-to-pulse timing jitter is an essential parameter of the detector, determining the temporal resolution of the entire setup. It was shown that the intrinsic jitter of the SSPD (when light is delivered to the SSPD in free space) is 18 ps including jitter of the read-out electronics [7]. That experiment had its goal to measure the minimum achievable jitter. Thus, the light was delivered into the optical cryostat as a short-distance free space propagating beam and low-noise electronics was used. The jitter value was obtained by direct measurement of delay between the laser trigger pulse

and the SSPD response. Recently jitter for a $10 \mu\text{m} \times 10 \mu\text{m}$ SSPD made from 3.5 nm thick NbN film was measured in several independent experiments. In [35] 37 ps jitter was reported for a SSPD coupled to a 2 m long single-mode optical fiber and ≈ 60 ps for a SSPD coupled to a multi-mode fiber. In both cases jitter was measured as delay between the laser trigger and the SSPD response. The difference in the jitter values was attributed to the long optical and electrical cables as well as to the dispersion in the multi-mode fiber. In [16] a 74 ps timing jitter was reported for such a fiber-coupled system measured in a different way, i.e. by a photon correlation technique. This value includes all electronic jitter which is evaluated to be under 30 ps. Finally, in [29] 16 ps timing jitter was measured for a parallel wire SSPD with a technique similar to the one described in [35], i.e. jitter was derived from a histogram of delay between the SSPD response and the laser trigger by the standard feature of the oscilloscope. In comparison, the timing jitter of InGaAs APD is typically in the order of 200–300 ps. In this system we used a standard single-wire SSPD. For them, the 100 ns separation between two subsequent pulses is sufficient to allow signal relaxation to

zero for the 10 MHz rate [16]. It is worth noting that in InGaAs APDs a deadtime of a few μ s typically reduces the maximum counting frequency to well below 1 MHz. The SSPD hence presents a maximum counting frequency more than an order of magnitude larger than APDs. This could be further improved by a better matching of the amplifier bandwidth, and by using meander structures with lower kinetic inductance (see Section 4 in this paper).

7. Conclusion

In conclusion, the SSPD is a device of choice for state-of-the-art photonics experiments. The SSPD exhibits up to 30% quantum efficiency in visible and near infrared. Recently we developed a new generation of the SSPD that exhibits a 150 ps response time giving a way to achieve GHz counting rates. Simultaneously these devices are capable of photon number resolving: up to four simultaneously absorbed photons are clearly resolved.

Acknowledgement

This work was supported by EU FP6 STREP 'SINPHONIA' (contract number NMP4-CT-2005-16433), Russian Agency on Science and Innovation contract 02.740.11.0228 and Russian Foundation for Basic Research Grant 09-02-12364.

References

- [1] Cova, S.; Ghioni, M.; Lacaita, A.; Samori, C.; Zappa, F. *Appl. Opt.* **1996**, *35*, 1956–1976.
- [2] Zappa, F.; Lacaita, A.; Cova, S.; Webb, P. *Opt. Lett.* **1994**, *19*, 846–848.
- [3] Rosenberg, D.; Lita, A.; Miller, A.; Nam, S.W. *Phys. Rev. A* **2005**, *71*, 061803(R).
- [4] Gol'tsman, G.; Okunev, O.; Chulkova, G.; Lipatov, A.; Semenov, A.; Smirnov, K.; Voronov, B.; Dzardanov, A.; Williams, C.; Sobolewski, R. *Appl. Phys. Lett.* **2001**, *79*, 705–707.
- [5] Gol'tsman, G.; Minaeva, O.; Korneev, A.; Tarkhov, M.; Rubtsova, I.; Divochiy, A.; Milostnaya, I.; Chulkova, G.; Kaurova, N.; Voronov, B.; Pan, D.; Cross, A.; Pearlman, A.; Komissarov, I.; Slys, W.; Sobolewski, R. *IEEE T. Appl. Supercon.* **2007**, *17* (1), 246–251.
- [6] Korneev, A.; Kouminov, P.; Matvienko, V.; Chulkova, G.; Smirnov, K.; Voronov, B.; Gol'tsman, G.; Currie, M.; Lo, W.; Wilsher, K.; Zhang, J.; Slys, W.; Pearlman, A.; Verevkin, A.; Sobolewski, R. *Appl. Phys. Lett.* **2004**, *84*, 5338–5340.
- [7] Verevkin, A.; Pearlman, A.; Slys, W.; Zhang, J.; Currie, M.; Korneev, A.; Chulkova, G.; Okunev, O.; Kouminov, P.; Smirnov, K.; Voronov, B.; Gol'tsman, G.; Sobolewski, R. *J. Mod. Opt.* **2004**, *51*, 1447–1458.
- [8] Slys, W.; Wegrzecki, M.; Bar, J.; Gorska, M.; Zwiller, V.; Latta, C.; Bohi, P.; Milostnaya, I.; Minaeva, O.; Antipov, A.; Okunev, O.; Korneev, A.; Smirnov, K.; Voronov, B.; Kaurova, N.; Gol'tsman, G.; Pearlman, A.; Cross, A.; Komissarov, I.; Verevkin, A.; Sobolewski, R. *Appl. Phys. Lett.* **2006**, *88*, 261113.
- [9] Zinoni, C.; Alloing, B.; Li, L.H.; Marsili, F.; Fiore, A.; Lunghi, L.; Gerardino, A.; Vakhtomin, Y.B.; Smirnov, K.V.; Gol'tsman, G.N. *Appl. Phys. Lett.* **2007**, *91*, 031106.
- [10] Hadfield, R.; Stevens, M.; Gruber, S.; Miller, A.; Schwall, R.; Mirin, R.; Nam, S.W. *Opt. Express* **2005**, *13*, 10846.
- [11] Takesue, H.; Nam, S.W.; Zhang, Q.; Hadfield, R.; Honjo, T.; Tamaki, K.; Yamamoto, Y. *Nat. Photon.* **2007**, *1*, 343–348.
- [12] Hadfield, R.; Habif, J.; Schlafer, J.; Schwall, R.; Nam, S.W. *Appl. Phys. Lett.* **2006**, *89*, 241129.
- [13] Robinson, B.; Kerman, A.; Dauler, E.; Barron, R.; Caplan, D.; Stevens, M.; Carney, J.; Hamilton, S.; Yang, J.; Berggren, K. *Opt. Lett.* **2006**, *31*, 444–446.
- [14] Stevens, M.; Hadfield, R.; Schwall, R.; Nam, S.W.; Mirin, R.; Gupta, J. *Appl. Phys. Lett.* **2006**, *89*, 031109.
- [15] Stevens, M.; Hadfeld, R.; Schwall, R.; Nam, S.W.; Mirin, R. *IEEE J. Sel. Top. Quant.* **2006**, *12*, 1255–1268.
- [16] Korneev, A.; Vachtomin, Y.; Minaeva, O.; Divochiy, A.; Smirnov, K.; Okunev, O.; Goltsman, G.; Zinoni, C.; Chauvin, N.; Balet, L.; Marsili, F.; Bitauld, D.; Alloing, B.; Lianhe, L.; Fiore, A.; L. Lunghi, A.G.; Halder, M.; Jorel, C.; Zbinden, H. *IEEE J. Sel. Top. Quant.* **2007**, *13*, 944–951.
- [17] Chen, J.; Altepeter, J.; Medic, M.; Lee, K.F.; Gokden, B.; Hadfield, R.; Nam, S.W.; Kumar, P. *Phys. Rev. Lett.* **2008**, *100*, 133603.
- [18] Halder, M.; Beveratos, A.; Gisin, N.; Scarani, V.; Simon, C.; Zbinden, H. *Nat. Phys.* **2007**, *3*, 692–695.
- [19] Gol'tsman, G.; Smirnov, K.; Kouminov, P.; Voronov, B.; Kaurova, N.; Drakinsky, V.; Zhang, J.; Verevkin, A.; Sobolewski, R. *IEEE Trans. Appl. Supercon.* **2003**, *13*, 192–195.
- [20] Cherednichenko, S.; Yagoubov, P.; Il'in, K.; Gol'tsman, G.; Gershenzon, E. Large Bandwidth of NbN Phonon Cooled Hot Electron Bolometer Mixers on Sapphire Substrates. *Proceedings of the 8th International Symposium on Space Terahertz Technology*, Cambridge, MA, USA, March 25–27, 1997.
- [21] Korneev, A.; Matvienko, V.; Minaeva, O.; Milostnaya, I.; Rubtsova, I.; Chulkova, G.; Smirnov, K.; Voronov, B.; Gol'tsman, G.; Slys, W.; Pearlman, A.; Verevkin, A.; Sobolewski, R. *IEEE Trans. Appl. Supercon.* **2005**, *15*, 571–574.
- [22] Anant, V.; Kerman, A.J.; Dauler, E.A.; Yang, J.K.W.; Rosfjord, K.M.; Berggren, K.K. *Opt. Express* **2008**, *16*, 10750.
- [23] Milostnaya, I.; Korneev, A.; Rubtsova, I.; Seleznev, V.; Minaeva, O.; Chulkova, G.; Okunev, O.; Voronov, B.; Smirnov, K.; Gol'tsman, G.; Slys, W.; Wegrzecki, M.; Guzewicz, M.; Bar, J.; Gorska, M.; Pearlman, A.; Kitaygorsky, J.; Cross, A.; Sobolewski, R. *J. Phys.: Conf. Ser.* **2006**, *43*, 1334–1337.

- [24] Rosfjord, K.; Yang, J.; Dauler, E.; Kerman, A.; Anant, V.; Voronov, B.; Goltsman, G.; Berggren, K. *Opt. Express* **2006**, *14*, 527–534.
- [25] Tarkhov, M.; Morozov, D.; Mauskopf, P.; Seleznev, V.; Korneev, A.; Kaurova, N.; Rubtsova, I.; Minaeva, O.; Voronov, B.; Gol'tsman, G. Single Photon Counting Detector for THz Radioastronomy. *Proceedings of the 17th International Symposium on Space Terahertz Technology*, Paris, France, May 10–12, 2006.
- [26] Zhang, J.; Slys, W.; Verevkin, A.; Okunev, O.; Chulkova, G.; Korneev, A.; Lipatov, A.; Gol'tsman, G.; Sobolewski, R. *IEEE Trans. Appl. Superconductivity* **2003**, *13*, 180–183.
- [27] Kerman, A.; Dauler, E.; Keicher, W.; Yang, J.; Berggren, K.; Gol'tsman, G.; Voronov, B. *Appl. Phys. Lett.* **2006**, *88*, 111116.
- [28] Tinkham, M. *Introduction to Superconductivity*; McGraw-Hill: New York, 1996.
- [29] Tarkhov, M.; Claudon, J.; Poizat, J.P.; Korneev, A.; Divochiy, A.; Seleznev, V.; Kaurova, N.; Voronov, B.; Gol'tsman, G. *Appl. Phys. Lett.* **2008**, *92*, 241112. <http://link.aip.org/link/?APL/92/241112>
- [30] Il'in, K.; Lindgren, M.; Currie, M.; Semenov, A.; Gol'tsman, G.; Sobolewski, R.; Cherednichenko, S.; Gershenzon, E. *Appl. Phys. Lett.* **2000**, *76*, 2752–2754.
- [31] Divochiy, A.; Marsili, F.; Bitauld, D.; Gaggero, A.; Leoni, R.; Mattioli, F.; Korneev, A.; Seleznev, V.; Kaurova, N.; Minaeva, O.; Gol'tsman, G.; Lagoudakis, K.G.; Benkhaoul, M.; Lévy, F.; Fiore, A. Superconducting Nanowire Photon-number-resolving Detector at Telecommunication Wavelengths. *Nat. Photon, Submitted for Publication*, 2008.
- [32] Marsili, F.; Bitauld, D.; Fiore, A.; Gaggero, A.; Leoni, R.; Mattioli, F.; Divochiy, A.; Korneev, A.; Seleznev, V.; Kaurova, N.; Minaeva, O.; Gol'tsman, G. *J. Mod. Opt.* **2009**, *56*, 334–344.
- [33] Korneev, A.; Divochiy, A.; Tarkhov, M.; Minaeva, O.; Seleznev, V.; Kaurova, N.; Voronov, B.; Okunev, O.; Chulkova, G.; Milostnaya, I.; Smirnov, K.; Gol'tsman, G. *J. Phys.: Conf. Ser.* **2008**, *97*, 012307.
- [34] Rosenberg, D.; Nam, S.W.; Miller, A.; Salminen, A.; Grossman, E.; Schwall, R.; Martinis, J. *Nucl. Instrum. Meth. Phys. Res. A* **2004**, *520*, 537–540.
- [35] Slys, W.; Wegrzecki, M.; Bar, J.; Grabiec, P.; Górka, M.; Zwiller, V.; Latta, C.; Böhi, P.; Pearlman, A.; Cross, A.; Pan, D.; Kitaygorsky, J.; Komissarov, I.; Verevkin, A.; Milostnaya, I.; Korneev, A.; Minayeva, O.; Chulkova, G.; Smirnov, K.; Voronov, B.; Gol'tsman, G.; Sobolewski, R. *J. Mod. Opt.* **2007**, *54*, 315–326.